Provided for non-commercial research and education use.
Not for reproduction, distribution or commercial use.

(This is a sample cover image for this issue. The actual cover is not yet available at this time.)

This article appeared in a journal published by Elsevier. The attached copy is furnished to the author for internal non-commercial research and education use, including for instruction at the authors institution and sharing with colleagues.

Other uses, including reproduction and distribution, or selling or licensing copies, or posting to personal, institutional or third party websites are prohibited.

In most cases authors are permitted to post their version of the article (e.g. in Word or Tex form) to their personal website or institutional repository. Authors requiring further information regarding Elsevier's archiving and manuscript policies are encouraged to visit:

http://www.elsevier.com/copyright

Chemical Engineering Journal 219 (2013) 335–345

Contents lists available at SciVerse ScienceDirect

Chemical Engineering Journal

journal homepage: www.elsevier.com/locate/cej

Experimental determination of mass transfer coefficients of volatile sulfur odorants in biofilter media measured by Proton-Transfer-Reaction Mass Spectrometry (PTR-MS)

Dezhao Liu [a], Rune Røjgaard Andreasen [b], Tjalfe Gorm Poulsen [b], Anders Feilberg [a,*]

[a] Department of Engineering, Faculty of Science and Technology, Aarhus University, Blichers Allé 20, Tjele 8830, Denmark
[b] Department of Chemistry, Environment and Biotechnology, Aalborg University, Sohngaardsholmsvej 57, Aalborg 9000, Denmark

HIGHLIGHTS

- ▶ A method of mass transfer coefficient determination in biofilter media was developed.
- ▶ PTR-MS supplied profile measurements in biofilter media for volatile sulfur odorants.
- ▶ Injection strategies were performed for optimization of breakthrough curves.
- ▶ Mass transfer was determined by PTR-MS data combined with computer modeling.

ARTICLE INFO

Article history:
Received 12 September 2012
Received in revised form 13 December 2012
Accepted 30 December 2012
Available online 11 January 2013

Keywords:
Mass transfer
Biological air filter
PTR-MS
Volatile sulfur compounds

ABSTRACT

Mass transfer from air to the liquid phase is an important process that may limit the efficiency of biological air filters used for abatement of odor from livestock production facilities. Mass transfer limitation is especially important for volatile sulfur compounds with relatively low aqueous solubility. A better understanding of limitations of mass transfer is therefore important in order to enhance the performance and design of biofilters. In this study, a method based on Proton-Transfer-Reaction Mass Spectrometry (PTR-MS) has been developed in combination with a developed model to determine the mass transfer coefficients of volatile sulfur compounds for selected packing material used in biofilters. PTR-MS was used to measure breakthrough curves for sulfur compounds with adequate sensitivity, time resolution and reproducibility. The overall mass transfer coefficient for the selected biofilter media was then estimated by fitting an advection–dispersion equation modified for mass transfer between the gas and liquid phases to the measured profile of individual sulfur compound. Different injection strategies were evaluated and an optimal measurement procedure was developed. The method was validated by comparison of mass transfer coefficients to literature values for toluene, which was used as a reference compound in this study. By applying the method to compounds with different Henry's law constants, the application range of the method was demonstrated regarding solubility in water. This study demonstrates a method for determination of mass transfer coefficients of sparingly soluble gaseous compounds for selected biofilter media by applying PTR-MS in combination with modeling.

© 2013 Elsevier B.V. All rights reserved.

1. Introduction

Biofilters has been recognized as suitable for treating volatile organic compounds with low concentrations and large flow rates [1]. In recent years, biofilters have also been increasingly used for treating odorous emissions from animal production facilities [2–5]. Those offending odorous compounds consist of several species including volatile sulfur contaminants such as hydrogen sulfide, methanethiol and dimethyl sulfide [6]. Compared to other technologies for odor reduction (e.g., slurry oxidation and chemical treatment [7]), biofilters are generally acknowledged as a cost-effective technology [2,8,9]. However, low removal efficiencies have been observed for volatile sulfur compounds present in the ventilation air to be treated [5,10]. Due to the high air velocity typically applied in an animal house ventilation system, short empty bed residence times (EBRTs) are common in order to reduce the pressure drop across the biofilter [2,4,11].Volatile organic sulfur compounds such as methanethiol or dimethyl sulfide have relatively low solubility in the aqueous phase in biofilters, which become a challenge when biofilters are used to remove those compounds from the ventilation air [12]. Since the mass transfer from the gas phase to the

* Corresponding author. Tel.: +45 8715 7647; fax: +45 8715 6000.
E-mail address: Anders.Feilberg@agrsci.dk (A. Feilberg).

1385-8947/$ - see front matter © 2013 Elsevier B.V. All rights reserved.
http://dx.doi.org/10.1016/j.cej.2012.12.088

liquid phase is one of the main factors influencing the performance of biological filters [13], the mass transfer resistance from the gas phase to the wet surface of the biofilter medium is thus considered as an important limitation for obtaining good removal of less water soluble compounds [14].

In order to enhance the performance and design of biofilters, a better understanding of the level and limitations of the mass transfer rates of volatile sulfur compounds is therefore important [13]. Although there are plenty of mass transfer correlations data obtained from wet scrubbers, they are not necessarily suitable for usage in biofiltration processes due to the large difference in superficial gas velocities or liquid velocities operated between biofiltration conditions and wet scrubbers [15]. Furthermore, most of the mass transfer data are obtained for oxygen (which is important for aerobic conditions) and those data cannot with certainty be expanded to be used for other compounds such as sulfur compounds in this study due to the difference in diffusion and partitioning coefficients. So far only limited experimental work has been done regarding mass transfer for packing materials used in biofilters [15,16]. Kim and Deshusses [15] performed a comprehensive investigation of gas-film (using carbon dioxide) and liquid-film (using oxygen) mass transfer coefficients measured in different operation conditions for commonly used packing materials in biofilters and biotrickling filters. Dorado et al. [16] demonstrated a method which could be used to evaluate the overall mass transfer coefficient of a realistic pollutant (toluene) instead of using CO_2. Other authors have also performed experimental measurements of overall mass transfer coefficients for toluene in biotrickling filters or biofilters with different conditions [14,17–19]. Hodge and Devinny evaluated a method for testing mass transfer constants and partition coefficients in biofilters using ethanol and CO_2 [20]. However, no systematic development has been performed regarding optimized determination of overall mass transfer constants for a range of target pollutants in biofilter media so far.

In this study, a method is developed for evaluation of overall mass transfer coefficients with the aid of Proton Transfer Reaction-Mass Spectrometry (PTR-MS) for measurements of pollutant breakthrough curves in combination with a numerical diffusion–dispersion model. Hydrogen sulfide (H_2S), Methanethiol (MT), dimethyl sulfide (DMS), dimethyl disulfide (DMDS) and dimethyl trisulfide (DMTS) were selected for the tests in this study as they represent significant components of typical malodorous air emitted from animal facilities and are sparingly soluble in water. Toluene was also included as a reference gas with respect to literature data since it is a commonly used model pollutant for mass transfer process investigation in biofilters and biotrickling filters [14,16,19]. Different contaminant tracer injection strategies were tested with respect for obtaining consistent breakthrough curves under identical experimental conditions. The measured breakthrough curves from different injection strategies were put into the numerical model and mass transfer coefficients were then optimized and compared to each other for validation of the method and internal comparison. Obtained mass transfer coefficient for toluene was compared to literature data available for demonstration of the method. Furthermore, a range of compounds with different solubilities were selected to investigate the application and limitation of the method regarding compounds with different Henry's law constants.

2. Materials and methods

2.1. Packing material

A commercially available material, fresh Leca® pellets (Lightweight Expanded Clay, diameter d = 8–10 mm), which was produced and provided by Saint-Gobain Weber A/S Randers, Denmark, was selected for the method establishment and validation in this study. This material was chosen due to its well defined particle size, relatively high specific surface area (a_e = 372 $m^2\ m^{-3}$ for Leca® 8–10 mm [21]) and no degradation over time. Also this material represents a wide range of both artificial and natural (stones, pebbles) granular biofilter materials. Leca® consists of porous rounded, particles and has a total porosity of 0.87–0.92 $m^3\ m^{-3}$ of which 55–70% are intra particle (internal) pores which are either very small or not connected with the external air filled pores and therefore do not conduct air.

Characterization of the packing material was carried out before usage. Mean dry bulk density (ρ_b = 0.25 g cm^{-3}) was determined in triplicates by filling a 20 L bucket to the edge with dry Leca®, dropping it three times from a height of 3–5 cm to achieve a stable packing, and subsequently adding additional material to fill the empty volume created during packing. The Leca® was then weighed. As Leca® is non-expanding when wetted ρ_b is constant regardless of water content (the quantity of water contained in Leca®, θ, $cm^3\ cm^{-3}$). The mean particle density (ρ_p = 0.39 g cm^{-3}) was obtained by the weight (M_{tot}, g) and particle volume for randomly selected 10 individual particles of the packing material assuming smooth surface and ellipsoid shape. The diameter of each particle was measured in three perpendicular locations (d_1,d_2 and d_3) starting with the widest part of the particle:

$$\rho_p = \frac{\sum_1^{10}(\frac{1}{6}\pi d_1 d_2 d_3)}{M_{tot}} \quad (1)$$

Thus ρ_b and ρ_p could be used to estimate the external air-filled porosity ε_{ex} ($m^3\ m^{-3}$) as below:

$$\varepsilon_{ex} = 1 - (\rho_b \rho_p^{-1}) \quad (2)$$

2.2. Experimental set-up

The experimental determination of mass transfer coefficients was performed in a lab-scale set-up as shown in Fig. 1. An adsorption column (stainless steel ventilation tube, 25 cm ID) packed with selected Leca® pellets (approximately 1 m high) was used for the experiment. Hence, the diameter-to particle diameter ratio was ensured to be higher than 10 to avoid wall effects [22]. As shown by the arrows in Fig. 1, ambient air was introduced via a blower (CUBUFAN 160 EC ventilation pump, Jenk, Brøndby, Denmark) and distributed evenly downwards through the biofilter column. The air flow rate was recorded by a data logger through a flow sensor (VA400 thermal mass flow sensor, CS instruments, Tannheim, Germany). Deionized water was pumped (by an Iwaki Metering pump C30, Iwaki pumps, Japan) to the top of the biofilter column (~35 cm above the packing), mixed with pressurized air (around 0.5 bar) and injected into the air stream against air flow direction through a jet nozzle (Hardi 1553-08, Nørre Alslev og Taastrup, Denmark) with a Syntal swivel (disk with two pin-holes helping to distribute the water spray; Hardi 1154, Nørre Alslev og Taastrup, Denmark). This was done to ensure adequate distribution of the water and to prevent dehumidification of the filter medium during measurements.

2.3. Experimental procedure

The packing material (Leca® pellets) was prepared as follows for each experiment: Before the usage, the material was wetted to its maximum water holding capacity by soaking in the deionized water for at least 3 days; drained for 1 h before use in experiments; soaked in water again after each day of experiments. The experiment was operated in co-current configuration at room

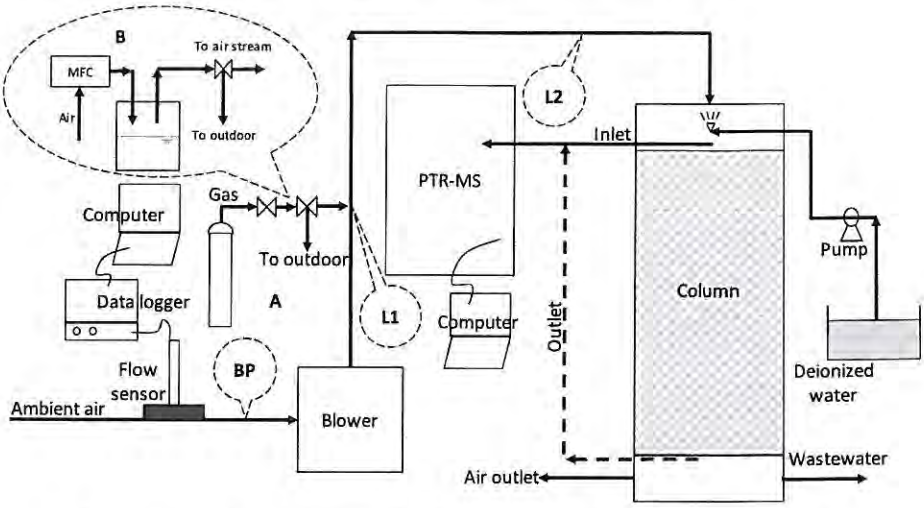

Fig. 1. Schematic of the mass transfer coefficient measurement set-up (MFC: mass flow controller).

temperature (20 ± 2 °C). The air flow rate was controlled at approximately 35 $m^3 h^{-1}$ with the EBRT ~5 s in the filter. The speed of the water flow (~1 L h^{-1}) was carefully controlled such that the biofilter weight was kept in the same level before and after each experiment (thus the humidity of the biofilter is kept in the same level for all experiments). It should be noted that although we used the term of 'biofilter' throughout the paper, the running conditions is more like a biotrickling filter although the water velocity is extremely low (5.1×10^{-4} cm s^{-1}). A pulse of single pollutant (H_2S, MT, DMS, DMDS, DMTS or Toluene) was introduced to the ambient air stream before going through the biofilter column. Three locations (Before Pump, BP; Location 1, L1; Location 2, L2; see Fig. 1) were chosen for introducing pollutant via manual injections or automatic injections. The automatic injections were controlled by solenoid valves (Burkert model 0124, Burkert, Germany). More details regarding injection strategies are described in Section 2.4. A high sensitivity PTR-MS (Ionicon Analytik, Innsbruck, Austria) was utilized to measure the profile of individual volatile compound in each experiment. Principles of the PTR-MS have been reviewed in extensively in review papers and will not be further discussed here [23–25]. The PTR-MS was run under standard conditions during all experiments. The drift tube temperature was set to 60 °C and the drift tube voltage was set to 600 V with a controlled drift tube pressure in the range of 2.1–2.2 mbar. The E/N number was maintained at ~135 Td during all experiments. The sensitivity of PTR-MS for measured compounds in this study was calculated using proton transfer rate constants [6] and the transmission curve was estimated by a mixture gas cylinder containing 14 aromatic compounds with m/z (mass to charge ratio) ranging between 79 and 181 (P/N 34423-PI, Restek, Bellefonte, Pennsylvania, USA). The humidity dependence calibration for hydrogen sulfide measured by PTR-MS was performed before and after the experiments using the method described by Feilberg et al. [6]. The dwell time for each compound was 100 ms during single experiment. Due to the short EBRT (~5 s) it was not possible to conduct profile measurements in multiple locations simultaneously with sufficient accuracy. Thus it was not possible to measure the breakthrough curves belonging to the same injection event at both the filter inlet (right above the packing) and outlet (right below the packing). To compensate for this, 5 consecutive inlet profiles, followed by 5 consecutive outlet profiles, and then followed by 3 consecutive inlet profiles were measured by PTR-MS for verifying the stability and reproducibility of the measured profiles. Duration of approximately 2.5 min was applied for a pause between two measured profiles in order to make sure the next profile started from the background level.

2.4. Injection strategies

With the purpose of getting the most stable breakthrough curves measured by PTR-MS and thereby to optimize the estimation of mass transfer coefficient, different injection strategies were performed in order to find the best injection location, the best injection mode (manual or automatic) and the best injection duration. Three kinds of injections (manual injection of a gas provided by a cylinder or from a Tedlar bag previously prepared, manual injection of a liquid pollutant, automatic injection of a gas) were performed at three injection locations (BP, L1 or L2; Fig. 1). L1 is located 0.7 m after the blower and 2.6 m before the inlet; BP is located 0.4 m before the blower; L2 is located 2.1 m after the blower and 1.2 m before the filter inlet. A full list of performed injection strategies is shown in Table 1. For manual injection of gas sample, sample (20 ml) from gas cylinder (1000 ppmv, Nitrogen based) which contains single compound (H_2S or MT; AGA A/S, Denmark) or from a pre-filled 10 L Tedlar bag (liquid compound was injected into the bag and evaporated before the test; DMS, DMDS, DMTS or toluene; all ⩾98%, Aldrich, Sigma–Aldrich) were implemented by using gas-tight syringes. Regarding manual injection of liquid samples, 1 μl of liquid compound (MT (67781, Aldrich, Sigma–Aldrich), DMS, DMDS, DMTS or toluene) were injected via one of three locations. For auto injection of gas samples, two 24 V solenoid valves (one 2-way valve followed by one

Table 1
Injection strategies for injection optimization.

Chemical	Auto injection						Manual injection					
	20 s			3 s			Gas			Liquid		
	BP	L1	L2	BP	L1	L2	BP	L1	L2	BP	L1	L2
H2S	Y	Y	Y	Y	Y	Y	Y	Y	Y	–	–	–
MT	Y	Y	Y	Y	Y	Y	Y	Y	Y	–	Y	–
DMS	Y	Y	Y	Y	Y	Y	–	Y	–	Y	Y	Y
DMDS	Y	Y	Y	Y	Y	Y	Y	Y	Y	–	Y	–
DMTS	Y	Y	Y	Y	Y	Y	Y	Y	Y	F	Y	–
Toluene	–	Y	Y	–	Y	Y	–	Y–	–	Y	–	

BP – Injection from location BP; L1 – Injection from location L1; L2 – Injection from location L2; Y – Injection performed; F – Injection failed.

3-way valve with which one way connecting to the 2-way valve, one way connecting to the injection location and another way connecting to the outdoor air) were used if gas cylinders were available (H_2S or MT; Fig. 1). The 24 V output is controlled by the external device interfaces (24 V) from the PTR-MS and thus synchronized with the measurements. The injection pressure maintained at 0.5 bars before the 2-way valve. When injection started, the 2-way valve was set from close condition to open condition and thus the pressure is released to reach the 3-way valve which was set to the way of reaching outdoor. After around 3.5 s, the 3-way valve was reset to the way reaching the injection location and thus the compound was injected to the air stream going towards the packed column. For compounds not available in gas cylinders (DMS, DMDS, DMTS or toluene), a headspace system (a constant, controlled air flow flushing the headspace of pure liquid compound) was used and followed by a 3-way valve controlled by the PTR-MS (Fig. 1; top-left corner, marked as B). Two dosage durations (3 s and 20 s; 3 s represents short dosage time but still has a reasonable but sharp peak of the profile, 20 s represents long dosage time with tailing after a flat peak of the profile), based on pretests of 1-butene and H_2S, were chosen for automatic injection in order to compare the duration sensitivity of profiles.

2.5. Application range test

In order to test the application of the method regarding compounds with different water solubility, volatile compounds with a range of Henry's law constants were carefully selected according to the detectability by PTR-MS and distribution of water solubility. The compounds which were chosen are listed below: 1-butene (1000 ppmv, AGA A/S, Denmark), Butanal (⩾99.0%, Fluka, Sigma–Aldrich), Octanal (99%, Aldrich, Sigma–Aldrich), Heptanal (>97%, Merck, Hohenbrunn, Germany), Nonanal (>98%, Merck, Hohenbrunn, Germany), Pentanal (97%, Aldrich, Sigma–Aldrich), Propanal (97%, Sigma–Aldrich), Ethanal (⩾99.5%, Fluka, Sigma–Aldrich), Hexanal (98%, Aldrich, Sigma–Aldrich), Decanal (>98%, Sigma, Sigma–Aldrich), 2-butanone (⩾99.0%, Sigma–Aldrich), Acetone (>99.0%, Merck, Hohenbrunn, Germany). Due to the large amount of fragmentations for some of the above compounds, fragmentations pattern for most compounds measured by PTR-MS were considered according to Kilpinen et al. [26] since the standard conditions were applied for both studies using the same type of PTR-MS. For pentanal, butanal and ethanal, fragmentation patterns were considered according to Schwarz et al. [27]. However, due to the limitation of dwell time of single cycle (which should not be too long), only one to three of the most abundant fragmentations were selected and then back calculation of concentration of single compound was performed according to the percentage of the selected fragmentations [26,27].

3. Theory

3.1. Modeling mass transfer in biofilters

Contaminants present in the biofilter gas phase will be subject to advection, diffusion, dispersion and mass exchange with the liquid phase during their transport through the biofilter material. By assuming that the water phase is stagnant while the air phase is moving, the combined action of these processes on the contaminant concentration in the gas phase is traditionally described as a function of time using the advection–dispersion equations as shown below [28]:

$$\frac{\partial C_g}{\partial_t} = D_p \frac{\partial^2 C_g}{\partial z_2} - u\frac{\partial C_g}{\partial z} - K_G a_e (C_g - C_l H) \tag{3}$$

where C_g is the gas phase concentration (mol m^{-3}); D_p is the dispersion–diffusion coefficient (m^2 s^{-1}); z is the filter depth (m); u is the pore air velocity (m s^{-1}); $K_G a_e$ is the overall volumetric air–water mass transfer coefficient (s^{-1}); C_l is the liquid phase concentration (mol m^{-3}); H is the dimensionless Henry's law constant (mol$_{gas}$ m$^{-3}_{gas}$/mol$_{liquid}$ m$^{-3}_{liquid}$ or –).

As no advective and diffusive/dispersive transport is assumed in the water phase the contaminant concentration as a function of time is given as:

$$\frac{\partial C_l}{\partial t} = K_G a_e (C_g - C_l H) \cdot \frac{\varepsilon_{ex}}{\theta_a} \tag{4}$$

where θ_a is the active water content (m^3 m^{-3}).

Estimation of the pore air velocity u is described below:

$$u = Q/(\pi \cdot r^2 \cdot \varepsilon_{ex}) \tag{5}$$

where Q is air flow rate (m^3 s^{-1}) and r is the radius of the filter cross section (m).

Pre-test of 1-butene showed that despite neglecting dispersion, the corresponding mass transfer was found extremely low. This indicated dispersion to be affecting the model results in an insignificant manner and thus was omitted from the biofilter model ($D_p = 0$). On the other hand, the active water content θ_a could not be determined independently and therefore was estimated together with $K_G a_e$ through the fitting process. It should be noted that θ_a is expected to be a function of the filter material characteristics and operation conditions but not the nature of the pollutants (e.g., H).

By using an explicit forward time and backward space finite difference scheme, Eqs. (3) and (4) could be solved in Microsoft Excel. Due to the embodied second-order numerical errors (numerical dispersion) by the type of numerical solution, a numerical correction scheme was applied to remove the second-order numerical errors. By giving appropriate time step ($\Delta t = 0.005$ s) and spatial step ($\Delta z = 0.04$ m) together with the initial values of concentrations (Eq. (6)) and initial estimated parameters, Eqs. (3) and (4) were solved numerically and a fitting curve for the outlet concentration could be then obtained from the inlet concentration (as input).

The initial concentrations in the fitting process were estimated as below:

$$\left.\begin{aligned} C_g(z_0, t_0) &= C_g(inlet_{measure,t_0}) \\ C_g(z_0 + \Delta z, t_0) = C_g(z_0 + 2\Delta z, t_0) &= \cdots C_g(outlet_{fit}, t_0) \\ &= \tfrac{1}{10}\sum_{i=0}^{9} C_g(outlet_{measure}, t_{0+i}) \\ C_g(z_0 + t_0) = C_l(z_0 + \Delta z, t_0) &= \cdots C_l(outlet_{fit}, t_0) \\ &= \tfrac{1}{10H}\sum_{i=0}^{9} C_g(outlet_{measure}, t_{0+i}) \end{aligned}\right\} \tag{6}$$

where z_0 is inlet ($z = 0$); t_0 is the starting time of the outlet profile and also the starting time of the fitting process ($t = 0$); $C_g(outlet_{measure}, t_{0+i})$ is the gas concentration at the ith point of the measured outlet profile.

The fitting curve was then optimized by minimization of the root mean square error (RMSE) between the fitted curve and measured outlet concentration:

$$\text{RMSE} = \sum [C_g(outlet_{measure}, t_i) - C_g(outlet_{fit}, t_i)]^2 \tag{7}$$

This was done through a least-squares method and only the decline part of the curve was fitted (from the observed maximum concentration to the point where the measured outlet concentration was less than 1% of the maximum concentration). The reason for only choosing the declining part of the curve for fitting is due to the fact that mass transfer generally has a stronger influence on the

declining part of the outlet breakthrough curve compared to the increasing part. Thus the optimized $K_G a_e$ and θ_a could be obtained through an iterative process based on Newton's method. The initial guess of both parameters were sequentially updated and Eqs. (3) and (4) were solved repeatedly until convergence occurred. Several initial guesses of $K_G a_e$ and θ_a (within 10 times difference) were tested in order to find the overall optimization point for the fitting curve.

3.2. Model sensitivity analysis

Sensitivity analysis can be used for assessing model performance by providing a general assessment of model precision or uncertainty in model inputs. Therefore sensitivity analysis investigates how much change of model output could be obtained by changing of model input. A dimensionless expression of sensitivity is the elasticity index, El_{IO}, which measures the relative change in output for a relative change in input, and could be defined as [29]:

$$El_{IO} = I_0/O(I_0)]SI_{IO} \quad (8)$$

$$SI_{IO} = \{|O(I_0) - O(I_d)]/(I_0 - I_d)| + |[O(I_0) - O(I_i)]/(I_0 - I_i)|\}/2 \quad (9)$$

SI_{IO}: sensitivity index; I_0: base input value; $O(I_0)$: base output value; I_d: decreased input value; $O(I_d)$: decreased output value; I_i: increased input value; $O(I_i)$: increased output value.

In this study, input was set to $K_G a_e$ and output was set to RMSE calculated from Eq. (7). The relative change of input applied was 10% of the numerical resolution of $K_G a_e$. The elasticity index was found to be similar when a different relative change of input applied (e.g., 30%). For the level of El_{IO}, one would expect higher is better and a value close to 1 would be satisfying since it shows the similar sensitivity of input and output.

3.3. Comparing different approaches for tracer injection

Breakthrough curves resulting from different tracer injection strategies were compared to select the optimal approach. The comparison was based on the use of the temporal moments of the breakthrough curves. The nth temporal moment of a concentration distribution at a location, z, is defined as [30]:

$$M_n = \int_0^\infty t^n C(z,t)dt \quad (10)$$

And the nth normalized moment of the distribution is defined as:

$$\gamma_n = \frac{M_n}{M_0} = \frac{\int_0^\infty t_n C(z,t)dt}{\int_0^\infty C(z,t)dt} \quad (11)$$

Analysis of the tracer breakthrough curves carried out in this paper will be based on the first four temporal moments ($n = 0$–3). The 0th temporal moment is the tracer mass injected and the 1st temporal moment is the mean residence time of a tracer compound in the filter. The 2nd and 3rd temporal moments represent the spread and the skewness of the resulting breakthrough curves, respectively.

4. Results and discussion

4.1. Injection optimization

Table 1 shows the injection strategies performed in this study for injection optimization and results are shown in Figs. 1–6. Temporal moments were first calculated for each breakthrough profile. Then the mean and standard deviation (STD) of the nth temporal moment (0th, 1st, 2nd, 3rd, respectively) were obtained based on the first 5 inlet profiles (inlet), 5 outlet profiles (outlet), or 8 inlet profiles (inlet, 5 + 3; 3 inlet profiles were measured after 5 outlet profiles). The relative standard deviation (RSD = $\frac{std}{mean} \times 100$) were chosen as an indicator in order to compare directly the precision of nth temporal moments from different injection methods. The

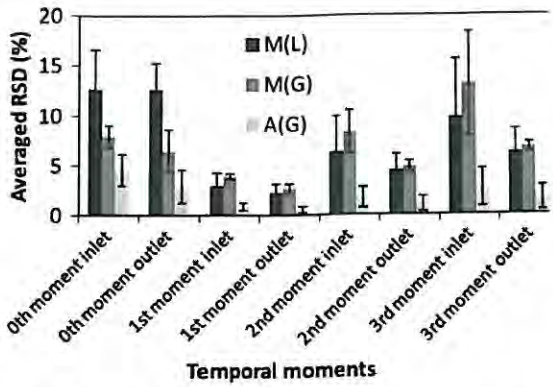

Fig. 2. Relative standard deviation of temporal moments for measured profiles from manual injection of gas (M(G)), from manual injection of liquid (M(L)) and from auto injection (of gas) (A(G)) averaged for all chemicals (sulfur compounds and toluene which were included for injection optimization; not including the additional compounds, e.g., acetone, heptanal, etc.) and all locations tested. For auto injection, both injections for 20 s and for 3 s are included.

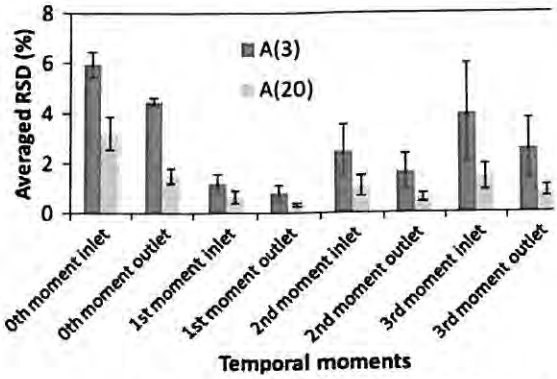

Fig. 3. Relative standard deviation of temporal moments for measured profiles from auto injection for 3 s (A(3)) and from auto injection for 20 s (A(20)) averaged for all chemicals (sulfur compounds and toluene) and all locations tested.

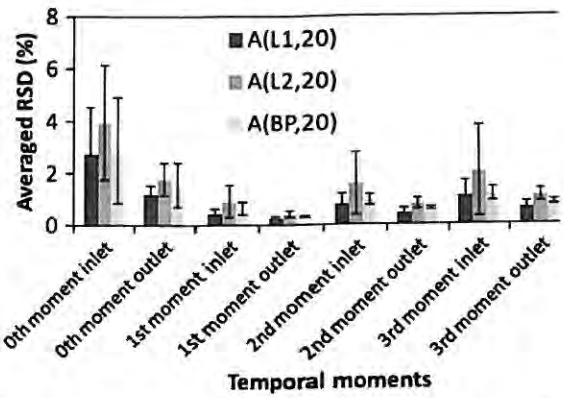

Fig. 4. Relative standard deviation of temporal moments for measured profiles from auto injection at location L1 for 20 s (A(L1,20)) and from auto injection at location L2 for 20 s (A(L2,20)) and from auto injection at location BP for 20 s (A(BP,20)) averaged for all chemicals tested (sulfur compounds and toluene).

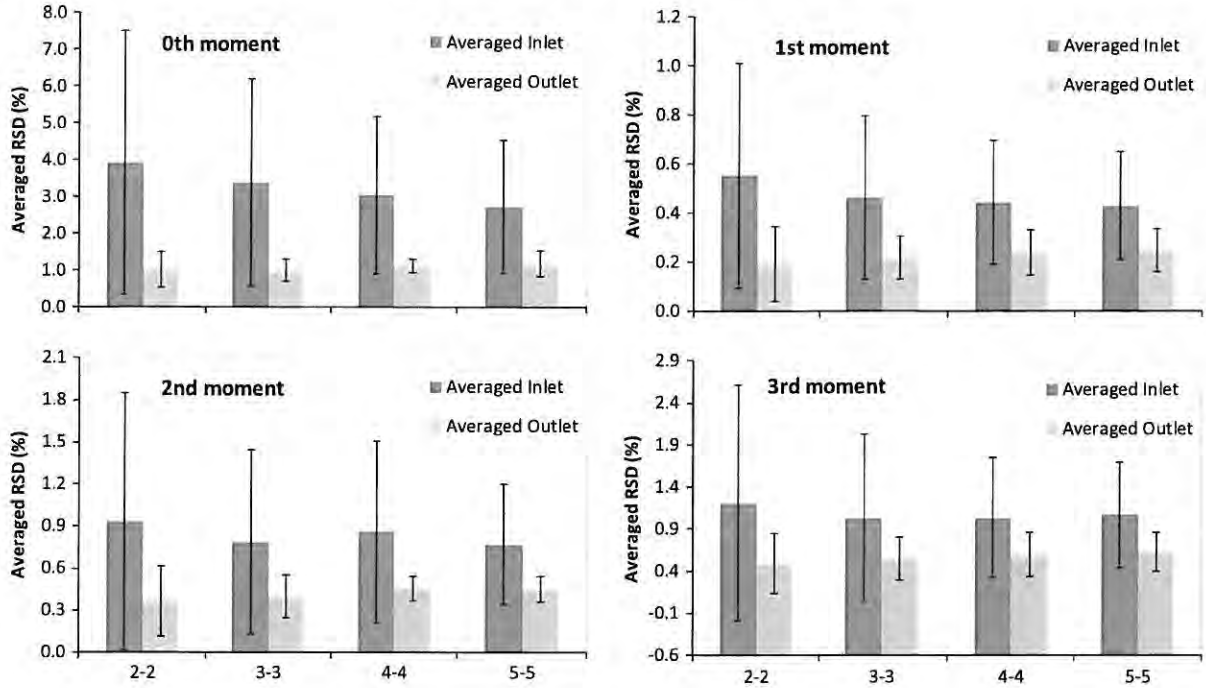

Fig. 5. Relative standard deviation of temporal moments for measured profiles from 2-2, 3-3, 4-4, 5-5 inlets and outlets averaged for all chemicals (sulfur compounds and toluene).

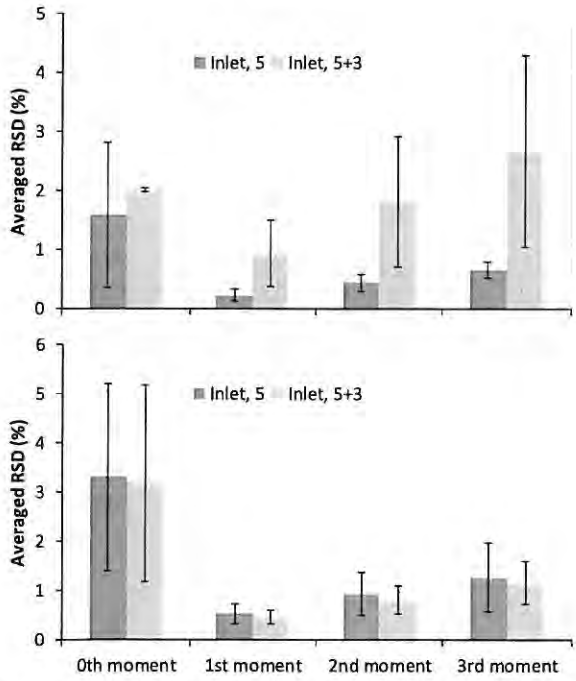

Fig. 6. Relative standard deviation of temporal moments for measured inlet profiles from 5 inlets (Inlet 5) and 5+3 inlets (Inlet 5+3) averaged for chemicals from gas cylinder sources (upper graph; H_2S and MT) and for chemicals from headspace sources (lower graph; DMS, DMDS, DMTS and Toluene). All profiles are from auto injection at location L1 for 20 s.

smaller values of RSD, the better precision of calculated *n*th temporal moments and thus more stable and repeatable measured profiles are obtained (e.g., see Fig. S1; Supplementary information). As shown in Figs. 2–6, RSD in this study stayed low for whatever the mode and the nature of the injections, even in the worst cases.

4.1.1. Influence of the kind of injections

When comparing manual injections of gas and liquid (Fig. 2), the variability of injected masses (0th moment) by gas injections is smaller compared to that by liquid injections. This may be due to the much smaller volume (20,000 times smaller) of injected liquid (1 μl) than the amount of injected gas (20 ml). On the other hand, the variability of residence time, spread, skewness (1st, 2nd, 3rd temporal moments, respectively) by gas injection are slightly higher than those by liquid injection manually. Due to the much smaller volume of liquid by manual injection, the injection duration was expected to be shorter than that by gas injection (thus more stable injections of liquid were expected regarding residence time, spread and skewness of the profiles). However, the liquid injected need to be evaporated and mixed with the air flow and this may need some time and introduce extra error. It should be noted that the injection of liquid DMTS at location BP was failed (Table 1) since both inlet and outlet profiles formed small peaks and very long tailings. This may be partly due to the low evaporation rate (less volatile) of liquid DMTS and longer time needed for evaporation after injecting into the air flow. In addition, the soundproofing foam (a few centimeter thick) used in the blower which might contain air bubbles inside, which will most likely act as adsorption material with adsorption–desorption of compound passing through. Overall, the manual injection of gas and liquid gave similar level of reproducibility of breakthrough profiles.

On the other hand, variability for auto injections (of gas) is much smaller than that for manual injections (of gas) for all temporal moments (Fig. 2). In theory, the masses (0th moment) injected by manual injections were expected to be consistent since the manual injections were performed by the same person carefully. The results indicated that auto injections gave lower variability of injected masses than that by manual injections no matter how good the manual injections were performed. Further, the injection speed and the duration by manual injections may cause potential in-consistency regarding residence time, spread and skewness of the profiles when compared to auto injections. In total auto injections performed much better than manual injections.

4.1.2. Influence of the injection duration

When considering dosage duration for auto injections, longer dosage (20 s dosage) gave lower variability for all temporal moments than shorter dosage (3 s dosage) (Fig. 3). Due to the higher masses dosed by 20 s dosage, it was expected that the dosed masses (0th moment) gave lower variability. On the other hand, the response time (approximately 10–20 ms, Burkert technical data, Measured at valve outlet of 6 bar) of the 3-way valve could be a limiting factor for 3 s dosage since it can influence the injection duration and starting time of the dosage. Therefore the 3 s dosage may result higher in-consistency regarding residence time, spread and skewness of the profiles.

4.1.3. Influence of the injection location

In Fig. 4, the RSD of the temporal moments were compared for auto injections for 20 s regarding different injection locations (L1, L2, BP). In total injections at L1 and BP have lower variability for temporal moments than injections at L2. Since L2 was located only 1.2 m before the packing and thus the dosed gas chemical may not have enough time to distribute properly in the air stream. Further, the response time (around 10–20 ms) of the 3-way valve could be another limiting factor which may give more influence on injections at L2 regarding the injection duration and starting time of the dosage. On the other hand, injections at L1 gave slightly lower variability for temporal moments than injections at BP. Due to the soundproofing foam used in the blower, the adsorption–desorption effect on compound passing through may exist and may influence the consistency of breakthrough profiles.

4.1.4. Number of injections required

Up to now, the best injection method seems to be the auto injection at location L1 for 20 s. Since all comparisons above were based on the first 5 inlet profiles and 5 outlet profiles, then the question is that could we reduce the number of injections in order to save time but still get same level of consistency of the breakthrough profiles? Another question is if there is any change or drifting of the last 3 inlet profiles (after 5 outlet profiles) when compare to the first 5 inlet profiles? In order to answer the first question, the RSD of the temporal moments for measured profiles (auto injection, L1, 20 s) from the first 2-2, 3-3, 4-4, 5-5 inlets and outlets were compared to each other (Fig. 5). As can be seen that the dosed masses (0th moment) and residence time (1st moment) for inlet profiles had lower variability when more inlet profiles were included but no much difference were observed for spread and skewness of the inlet profiles. On the other hand, RSD of the temporal moments from the outlet profiles seems to be independent on number of profiles included. Thus, the conclusion for this question would be that the number of inlet profiles should remain in order to get more consistent breakthrough profiles but the number of outlet profiles may be reduced down to 3 profiles in order to save time.

Fig. 6 shows the comparison of RSD for the temporal moments from the first 5 inlet profiles and from the first 5 plus the last 3 inlet profiles (after 5 outlet profiles). For chemicals from the gas cylinder sources (H_2S and MT; upper graph in Fig. 6), injected masses (0th moment) are kept consistent between the first 5 inlet profiles and 5 + 3 inlet profiles. However, the residence time, spread, skewness seem to be drifted for the last 3 inlet profiles since the variability of the 1st, 2nd, 3rd temporal moments from the 5 + 3 inlet profiles dramatically higher from that from the first 5 inlet profiles. For chemicals from the headspace source (DMS, DMDS, DMTS and Toluene; lower graph in Fig. 6), on the contrary, all temporal moments are kept consistent between the first 5 inlet profiles and 5 + 3 inlet profiles. The reason for the different performance between different sources may be due to the difference of the injection control. For headspace sources, only one 2-way valve was applied while keeping a constant flow flushing through the headspace system during single experiment (5 inlet + 5 outlet + 3 inlet). For cylinder sources, on the other hand, one 2-way valve followed by one 3-way valve was applied and no constant flow were applied in order to save gas and to avoid pressure pulse. Thus the drifting may be due to the lack of the constant flow during the experiment and a system with a constant flow (e.g., controlled by a mass flow controller) together with a 2-way valve (automatic controlled by PTR-MS) is therefore recommended for consistent breakthrough profiles experiment. However, the procedure of 5 inlets followed by 3 to 5 outlets and followed by 3 inlets were kept for injections of chemicals from cylinder source in this study due to the fact that the system of 2-way valve followed by 3-way valve was applied in order to save gas.

4.1.5. Conclusions

Above all, auto injection of gas compound at location L1 for 20 s gave the most consistent breakthrough profiles. In conclusion, the injection procedure could be reduced to 5 inlets followed by 3–5 outlets for gas compounds using headspace sources. For gas compounds from gas cylinders, the procedure of 5 inlets followed by 3–5 outlets and followed by 3 inlets are recommended due to the usage of the system containing 2-way valve followed by 3-way valve in order to save gas during pause.

4.2. Mass transfer coefficient estimation

By using the fitting procedure described in Section 3.1, K_Ga_e can be obtained for specific compound measured by PTR-MS under the operation condition of this study. For all injection strategies performed in this study (Table 1), averaged inlet (from 8 inlet profiles) and outlet profiles (from 5 outlet profiles) together with measured air flow rates were used as inputs for the fitting process. Obtained K_Ga_e were summarized and shown in Table 2. At the same time of fitting K_Ga_e, θ_a were also obtained through the numerical resolutions as shown in Fig. S2. Obtained θ_a were basically close to each other for different measured pollutants and this confirmed that θ_a is not dependent on the nature of the pollutants. Fig. 7 shows some example profiles of average measured inlet, average measured outlet and fitted outlet for DMS under different injection strategies.

The "goodness of fit" was indicated by the coefficient of determination (R^2) for non-linear least-square fittings as shown in Eq. (12). The R^2 was calculated both for the whole curves and for the

Table 2
Averaged mass transfer coefficients K_Ga_e (RSD) by different injection strategies.

Chemical	Auto injection		Manual injection	Location		
	20 s	3 s		BP	L1	L2
H2S	0.07(31)	0.15(33)	0.13(13)	0.09(41)	0.14(30)	0.14(44)
Toluene	0.06(48)	0.09(40)	0.12(18)	(–)	0.09(47)	0.08(17)
MT	0.13(41)	0.17(60)	0.12(26)	0.14(34)	0.08(43)	0.19(35)
DMS	0.12(16)	0.16(43)	0.17(10)	0.09(30)	0.16(15)	0.17(30)
DMDS	0.24(15)	0.26(11)	0.32(17)	0.26(9)	0.29(19)	0.28(32)
DMTS	0.28(3)	0.35(11)	0.39(12)	0.32(9)	0.34(17)	0.37(24)

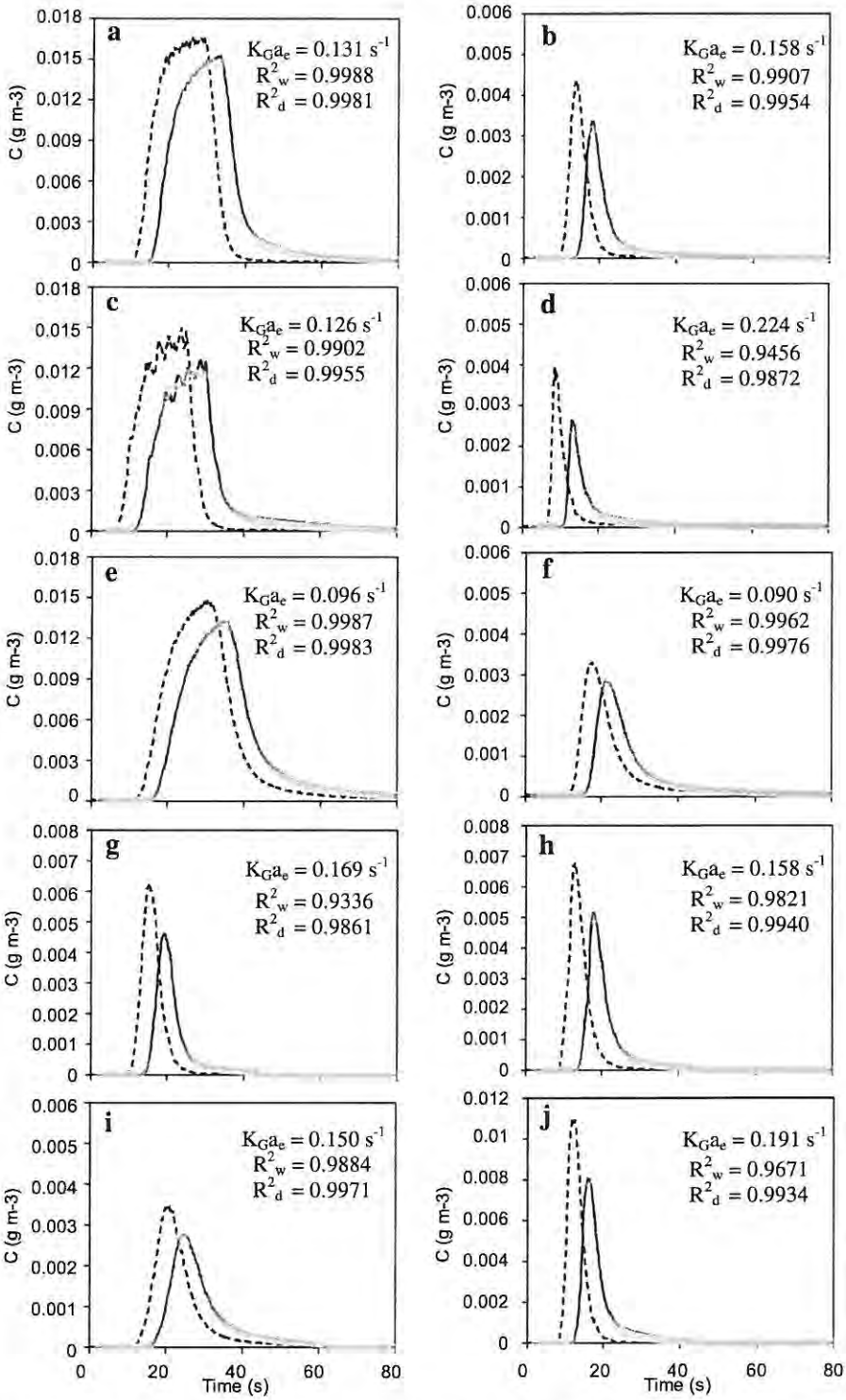

Fig. 7. Examples of profiles of measured inlet (—), measured outlet (○) and simulated outlet (▬) for DMS by different injection strategies. (a) automatic injection, L1, 20 s; (b) automatic injection, L1, 3 s; (c) automatic injection, L2, 20 s; (d) automatic injection, L2, 3 s; (e) automatic injection, BP, 20 s; (f) automatic injection, BP, 3 s; (g) manual injection, liquid, L1; (h) manual injection, liquid, L2; (i) manual injection, liquid, BP; (j) manual injection, gas, L1; R^2_w: The coefficient of determination between the whole curves of simulated outlet and measured outlet profiles; R^2_d: The coefficient of determination between the decline part of the simulated outlet and measured outlet profiles.

decline part of the curves since the fitting process was performed only for the decline part of the curve.

$$R^2 = 1 - \frac{SSE}{SST} = 1 - \frac{\sum_{i=1}^{n}(y_i - yf_i)^2}{\sum_{i=1}^{n}(y_i - \bar{y})^2} \quad (12)$$

As shown in Fig. 7, obtained R^2 for all the injection ways are high with the minimum R^2 value of all performed fitting equal to 0.9861 (for the decline part). Further, regardless of the difference of injection duration, mode, location and phase, obtained K_Ga_e are reasonably close to each other. This internal comparison

Table 3
Comparison of measured mass transfer coefficients (K_Ga_e) for toluene in biofilters/biotrickling filters.

Packing material	K_Ga_e (s^{-1})	Air velocity ($m\ s^{-1}$)	Liquid velocity ($cm\ s^{-1}$)	Refs.
Steel pall rings	0.0115–0.070	0.0044–0.022	0.092–0.131	[17]
Polypropylene rings	0.001–0.01	0.422–1.502	0.7–1.4	[18]
Lava rock	0.0115–0.214	0.0067–0.112	0.056	[16]
Clay pellets	0.0115–0.166	0.0067–0.112	0.056	[16]
Dixon rings	0.0123–0.459	0.0067–0.112	0.056	[16]
Polyurethane foam	0.0135–0.287	0.0067–0.112	0.056	[16]
Polyurethane foam	0.0397–0.127	0.0159–0.114	0.017	[19]
LECA 2–4 mm	0.036	0.032–0.037	7.7E–05	[14]
LECA 8–10 mm	0.087 ± 0.034	0.198	5.1E–04	This study

Table 4
List of compounds for application range test of mass transfer coefficient measurement.

Compound	H (–)[a]	STD_H[b]	K_Ga_e (s^{-1})	STD[d]	m/z[e]	EI_{10}[f]
1-Butene	1.0E+01	(–)	0.0015[c]	(–)	57	0.004
H_2S	3.9E–01	7.3E–02	0.120	0.047	35	1.00
Toluene	2.5E–01	3.8E–02	0.087	0.034	93	1.01
MT	1.4E–01	4.5E–02	0.140	0.064	49	1.57
DMS	7.5E–02	7.1E–03	0.149	0.044	63	1.97
Decanal	6.7E–02	(–)	0.131	(–)	83, 92	0.13
DMDS	4.8E–02	4.4E–03	0.277	0.056	95, 79	1.94
Nonanal	3.6E–02	6.7E–03	0.204	(–)	69, 83, 55	0.92
DMTS	3.1E–02	4.9E–04	0.341	0.058	127	2.02
Octanal	2.1E–02	1.4E–03	0.334	(–)	69, 41, 111	1.04
Heptanal	1.2E–02	9.5E–04	0.320	(–)	55, 97	1.30
Hexanal	8.5E–03	2.5E–04	0.420	(–)	55, 83	1.83
Pentanal	6.2E–03	2.0E–04	0.610	(–)	69, 41	1.90
Butanal	4.5E–03	3.5E–04	0.640	(–)	55, 73	0.85
Propanal	3.1E–03	(–)	0.787	(–)	59, 31	3.39
Ethanal	3.1E–03	5.4E–04	0.769	(–)	45	0.86
2-Butanone	2.2E–03	1.1E–04	(–)	(–)	73	(–)
Acetone	1.5E–03	1.2E–04	(–)	(–)	59	(–)

[a] Dimensionless Henry's law constant (H); the data are from NIST database and only measured values were included except for 1-butene and H_2S; for H_2S, MT, DMS and DMDS, the data from [12] were also included; For DMTS, the data is from [12].
[b] Standard deviation for dimensionless Henry's law constant.
[c] Value was obtained with low sensitivity.
[d] Standard deviation for mass transfer coefficients (K_Ga_e) including all injection strategies.
[e] Mass per charge ratio measured by PTR-MS.
[f] Elasticity index.

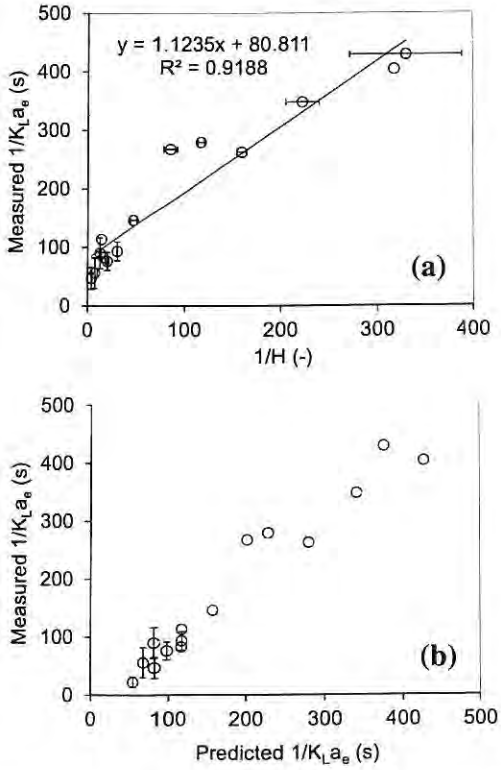

Fig. 8. The inverse of measured mass transfer coefficient K_La_e as a function of the inverse of dimensionless Henry's law constant H (a) and as a function of the inverse of predicted mass transfer coefficient K_La_e for selected compounds.

demonstrated the method used for determination of K_Ga_e in this study. However, there might be systematic errors among the different injection ways. For example, lower K_Ga_e were obtained from injections at BP than those from injections at L1 or L2 for all compounds except for MT (Table 2). Likewise, injections at L1 and L2 basically gave similar K_Ga_e for all compounds except for MT (Table 2). In addition, auto injections for 20 s gave smaller K_Ga_e than manual injections or auto injections for 3 s.

On the other hand, STD of K_Ga_e obtained from injections at BP was lower than these obtained from injections at L2, but comparable to those obtained from injections at L1. The higher in-consistency of obtained K_Ga_e from injections at L2 may be due to the higher in-consistency of injections at this location as discussed in Section 4.1 (Fig. 4). The lower K_Ga_e and lower STD of K_Ga_e obtained from injections at BP may be due to the adsorption–desorption happened in the blower where soundproofing foam was used. This adsorption and desorption can be clearly seen from the measured inlet profiles (longer tailing for inlet profiles which is more similar to outlet profiles) when compared to profiles from the other two locations (e.g., Fig. 7e vs. a and c). Whereas in some cases the STD (e.g., for DMDS and DMTS) by injections at BP were lower (than STD at L1), the number of measurements for the calculation of standard deviations were also smaller for injections at BP ($n = 3$) than for injections at L1 ($n = 4$) (Table 1). Moreover, auto injections for 20 s gave the best results regarding STD among the three injections modes (auto injections for 20 s, auto injections for 3 s and manual injections).

Table 3 shows the comparison of measured K_Ga_e of toluene in packing for biofilters or biotrickling filters from available literatures. Among all K_Ga_e data obtained from different packing materials, measured K_Ga_e in this study was comparable to most literature data. Due to the relatively high air velocity used in this study, higher K_Ga_e was expected. However, it should be noted that the increase of K_Ga_e may not be linearly related to the increase of air velocity and may possibly be 'saturated' by further increase of air velocity [31]. Moreover, the K_Ga_e is largely dependent on biofilter media characteristics which might provide the most explanation of the difference between measured values of K_Ga_e under similar operating conditions.

4.3. Method application range test

As discussed in Section 4.1, auto injection at L1 for 20 s was selected as the best injection method for breakthrough profiles

measurement. By applying the selected injection method, the application range of the established method for determination of K_Ga_e of compounds regarding solubility in water was demonstrated (Table 4). For compounds with very low water solubility such as 1-butene, it was found to be difficult to obtain the optimized K_Ga_e by the established method (very little change of RMSE using Eq. (7) in optimization process) due to the small amount of mass transferred from the gas phase to the water phase while passing through the packed column. As can be seen from Fig. S3a, there is no significant difference between the inlet profile and outlet profile for 1-butene due to the low air–water gas exchange and negligible dispersion. When analyzed through the sensitivity analysis, it can be seen that the elasticity index (EI_{IO}) for 1-butene is very low (0.006) compared to all the other compounds with much higher solubility measured in this study (all with $EI_{IO} > 0.85$ except for decanal with $EI_{IO} = 0.131$) (Table 4). The K_Ga_e of 1-butene showed in Table 4 could therefore only be considered as a rough estimation to the true K_Ga_e. Thus the upper limit of the application of the method in terms of H is considered to be around or slightly below 10. On the contrary, compounds with high solubility (e.g., 2-butanone) also had problems with fitting process due to the very small peak exhibited in the measured outlet (Fig. S3d). Although the optimized K_Ga_e is given in the figure, it was again only a rough estimation in this case. For compound such as ethanal with solubility somewhat lower than that of 2-butanone, the fitting was better but still with problems. Since the fitting process in this method only included the declining part of the curve, the extra peak in the simulated outlet curve show that some parts could not be simulated well by fitting only to the declining part of the curve (Fig. S3b). However, the fitting of the curve became much worse especially for the declining part when the fitting process included the whole curve (Fig. S3c). Therefore the lower limit of the H is estimated to be around 0.003 (–) for application of the method presented in this study.

As shown in Table 4, there is a decrease of K_Ga_e by the increased H for the selected compounds in this study. By using the well-known expression of K_La_e ($K_La_e = H * K_Ga_e$, s^{-1}) related to gas-phase mass transfer coefficient (k_Ga_e, s^{-1}) and liquid-phase mass transfer coefficient (k_La_e, s^{-1}) (Eq. (13)), the reverse of K_La_e can be presented as a function of $1/H$ as shown in Fig. 8a. Thus the values of k_La_e, k_L, k_G and k_Ga_e can be estimated from the slope and the origin of the regression line in Fig. 8a.

$$\frac{1}{K_La_e} = \frac{1}{k_La_e} + \frac{1}{Hk_Ga_e} \tag{13}$$

However, the above obtained values are only approximate since k_L ($m\,s^{-1}$) and k_G ($m\,s^{-1}$) depend on the nature of the pollutants. On the other hand, k_L and k_G can be estimated by Higbie penetration theory [32], which correlated the mass transfer coefficients for a compound i to their diffusion coefficients in the liquid ($D_{i,L}$, $cm\,s^{-1}$) and gas phases ($D_{i,G}$, $cm\,s^{-1}$) (Eqs. (14) and (15)).

$$k_L^i = \sqrt{\frac{4}{\pi\tau_L}}\sqrt{D)i,L} \tag{14}$$

$$k_G^i = \sqrt{\frac{4}{\pi\tau_G}}\sqrt{D_{i,G}} \tag{15}$$

where τ_L and τ_G refer to the exposure time of compound i in the liquid and the gas phase, respectively. τ_L and τ_G are constant while the operating conditions (gas and liquid flow rates, temperature, etc.) are kept constant for a given material. The reverse of K_La_e for compound i can then be related to $D_{i,L}$ and $D_{i,G}$ as shown in Eq. (15).

$$\frac{1}{K_L^ia_e} = \sqrt{\frac{\pi\tau L}{4}}\frac{1}{a_e\sqrt{D_{i,L}}} + \sqrt{\frac{\pi\tau G}{4}}\frac{1}{a_eH\sqrt{D_{i,G}}} \tag{16}$$

Thus τ_L and τ_G can be estimated (to be 8600 and 20,000, respectively) numerically by comparing the predicted K_La_e through Eq. (15) and measured K_La_e in this study (Fig. 8b). Here the $D_{i,L}$ was estimated based on Hayduk–Laudie correlation and $D_{i,G}$ was estimated based on Fuller–Schettler–Giddings correlation [33]. Further, the liquid and gas side mass transfer resistant can be estimated through the predicted K_La_e through Eq. (15) based on the estimated τ_L and τ_G, as shown in Table S1. The relative mass transfer resistance indicated that although the mass transfer of more volatile sulfur compounds (e.g., H_2S) is controlled by the liquid-phase mass transfer, the mass transfer of less volatile sulfur compounds (e.g., DMTS) is controlled by mass transfer from both phases.

5. Conclusions

In this study, a method for determination of mass transfer coefficients of air contaminants (volatile sulfur compounds) in biofilters has been developed and validated based on Proton-Transfer-Reaction Mass Spectrometry (PTR-MS) in combination with a developed model. PTR-MS was used to provide inlet and outlet profiles which were modeled using the advection–dispersion equation modified for mass transfer between gas phase and liquid phase in biofilters. By fitting the measured profiles of the sulfur compounds, the overall mass transfer coefficients were estimated. Different compound injection strategies were performed for optimization and internal demonstration of the method regarding ways of injection, dosage and injection locations. An injection procedure of 5 inlets followed by 3–5 outlets is recommended if only one 3-way valve is used, and a procedure of 5 inlets followed by 3–5 outlets and followed by 3 inlets are recommended if a 2-way valve followed by a 3-way valve are used. Toluene was used as a model contaminant for validation of the method and comparison of mass transfer coefficients to literatures. The application of the method to compounds with different Henry's law constant validated the method with a range of compounds regarding water solubility. This study demonstrates that it is possible and relevant to estimate mass transfer coefficients in biofilters for specific air contaminants by using PTR-MS in combination with modeling.

Acknowledgments

This study was funded by a grant from the Danish Strategic Research Council to the Project Cost-Effective Biofilter for Odour Nuisance Abatement for intensive pig production (CEBONA, Grant No. 2104-08-0017).

Appendix A. Supplementary material

Supplementary data associated with this article can be found, in the online version, at http://dx.doi.org/10.1016/j.cej.2012.12.088.

References

[1] J.S. Devinny, M.A. Deshusses, T.S. Webster, Biofiltration for Air Pollution Control, Lewis Publishers, Boca Raton, 1999. pp. 5–22.
[2] R.W. Melse, N.W.M. Ogink, Air scrubbing techniques for ammonia and odor reduction at livestock operations: review of on-farm research in the Netherlands, Trans. ASAE 48 (2005) 2303–2313.
[3] T.L. Jensen, M.J. Hansen, A biotrickling filter for removing ammonia and odour in ventilation air from a unit with growing-finishing pigs, in: Proc. Workshop on Agricultural Air Quality: State of the Science, North Carolina State Univ., Raleigh, 2006.
[4] L. Chen, S.J. Hoff, J.A. Koziel, L.S. Cai, B. Zelle, G. Sun, Performance evaluation of a wood-chip based biofilter using solid-phase microextraction and gas

chromatography-mass spectroscopy-olfactometry, Bioresour. Technol. 99 (2008) 7767–7780.
[5] A. Feilberg, A.P.S. Adamsen, S. Lindholst, M. Lyngbye, A. Schäfer, Evaluation of biological air filters for livestock ventilation air by membrane inlet mass spectrometry, J. Environ. Qual. 39 (2010) 1085–1096.
[6] A. Feilberg, D. Liu, A.P.S. Adamsen, M.J. Hansen, K. Jonassen, Odorant emissions from intensive pig production measured by online proton-transfer-reaction mass spectrometry, Environ. Sci. Technol. 44 (2010) 5894–5900.
[7] D. Liu, A. Feilberg, A.P.S. Adamsen, K.E. Jonassen, The effect of slurry treatment including ozonation on odorant reduction measured by in-situ PTR-MS, Atmos. Environ. 45 (2011) 3786–3793.
[8] D.H. O'Neill, I.W. Stewart, V.R. Phillips, A review of the control of odour nuisance from livestock buildings: Part 2, The costs of odour abatement systems as predicted from ventilation requirements, J. Agric. Eng. Res. 51 (1992) 157–165.
[9] L. Chen, S.J. Hoff, Mitigating odors from agricultural facilities: a review of literature concerning biofilters, Appl. Eng. Agric. 25 (2009) 751–766.
[10] M.J. Hansen, D. Liu, L.B. Guldberg, A. Feilberg, Application of proton-transfer-reaction mass spectrometry to the assessment of odorant removal in a biological air cleaner for pig production, J. Agric. Food Chem. 60 (2012) 2599–2606.
[11] D. Liu, M.J. Hansen, L.B. Guldberg, A. Feilberg, Kinetic evaluation of removal of odorous contaminants in a three-stage biological air filter, Environ. Sci. Technol. 46 (2012) 8261–8269.
[12] D. Liu, A. Feilberg, A.M. Nielsen, A.P.S. Adamsen, PTR-MS measurement of partition coefficient of reduced volatile sulfur compounds in liquids from biotricking filters, Chemosphere 90 (2013) 1396–1403.
[13] S. Kim, M.A. Deshusses, Understanding the limits of H_2S degrading biotrickling filters using a differential biotrickling filter, Chem. Eng. J. 113 (2005) 119–126.
[14] A.M. Nielsen, L.P. Nielsen, A. Feilberg, K.V. Christensen, A method for estimating mass-transfer coefficients in a biofilter from membrane inlet mass spectrometer data, J. Air Waste Manage. Assoc. 59 (2009) 155–162.
[15] S. Kim, M.A. Deshusses, Determination of mass transfer coefficients for packing materials used in biofilters and biotrickling filters for air pollution control. 1. Experimental results, Chem. Eng. Sci. 63 (2008) 841–855.
[16] A.D. Dorado, G. Rodriguez, G. Ribera, A. Bonsfills, D. Gabriel, J. Lafuente, X. Gamisans, Evaluation of mass transfer coefficients in biotrickling filters: experimental determination and comparison to correlations, Chem. Eng. Technol. 32 (2009) 1941–1950.
[17] A.R. Pedersen, E. Arvin, Removal of toluene in waste gases using a biological trickling filter, Biodegradation 6 (1995) 109–118.
[18] F. Heymes, P. Manno Demoustier, F. Charbit, J. Louis Fanlo, P. Moulin, Hydrodynamics and mass transfer in a packed column: case of toluene absorption with a viscous absorbent, Chem. Eng. Sci. 61 (2006) 5094–5106.
[19] R. Lebrero, J.M. Estrada, R. Munoz, G. Quijano, Toluene mass transfer characterization in a biotrickling filter, Biochem. Eng. J. 60 (2012) 44–49.
[20] D.S. Hodge, J.S. Devinny, Determination of transfer rate constants and partition coefficients for air phase biofilters, J. Environ. Eng. 123 (1997) 577–585.
[21] R.R. Andreasen, D. Liu, S. Ravn, A. Feilberg, T.G. Poulsen, Air–water mass transfer of sparingly soluble odorous compounds in granular biofilter media, Chem. Eng. J., 2013.
[22] A. Hoffmann, J.F. Maćkowiak, A. Górak, M. Haas, J.-M. Löning, T. Runowski, K. Hallenberger, Standardization of mass transfer measurements. A basis for the description of absorption processes, Chem. Eng. Res. Des. 85 (2007) 40–49.
[23] C.N. Hewitt, S. Hayward, A. Tani, The application of proton transfer reaction-mass spectrometry (PTR-MS) to the monitoring and analysis of volatile organic compounds in the atmosphere, J. Environ. Monit. 5 (2003) 1–7.
[24] J. de Gouw, C. Warneke, Measurements of volatile organic compounds in the earth's atmosphere using proton-transfer-reaction mass spectrometry, Mass Spectrom. Rev. 26 (2007) 223–257.
[25] R.S. Blake, P.S. Monks, A.M. Ellis, Proton-transfer reaction mass spectrometry, Chem. Rev. 109 (2009) 861–896.
[26] O. Kilpinen, D. Liu, A.P.S. Adamsen, Real-time measurement of volatile chemicals released by bed bugs during mating activities, PLoS One 7 (2012) e50981.
[27] K. Schwarz, W. Filipiak, A. Amann, Determining concentration patterns of volatile compounds in exhaled breath by PTR-MS, J. Breath Res. 3 (2009), art. no. 027002.
[28] J.D. Istok, Groundwater modeling by the finite element method, Amer. Geophysical Union, 1989.
[29] D.P. Loucks, E. van Beek, Water Resources Systems Plannning and Management, UNESCO Publishing, 2005. pp. 267–269.
[30] L. Pang, M. Goltz, M. Close, Application of the method of temporal moments to interpret solute transport with sorption and degradation, J. Contam. Hydrol. 60 (2003) 123–134.
[31] P.V. Roberts, G.D. Hopkins, C. Munz, A.H. Riojas, Evaluating two-resistance models for air stripping of volatile organic contaminants in a countercurrent, packed column, Environ. Sci. Technol. 19 (1985) 164–173.
[32] R. Higbie, The rate of absorption of a pure gas into a still liquid during short periods of exposure, Trans. Am. Inst. Chem. Eng. 35 (1935) 36–60.
[33] R.H. Perry, D.W. Green, J.O. Maloney, Perry's Chemical Engineers' Handbook, seventh ed., McGraw-Hill, Singapore, 1998.